High Performance Thermoelectric Tl_9BiTe_6 with an Extremely Low Thermal Conductivity

Bernd Wölfing,[1,2,*] Christian Kloc,[1] Jens Teubner,[1,2] and Ernst Bucher[1,2]
[1]*Bell Laboratories, Lucent Technologies, Mountain Avenue, Murray Hill, New Jersey 07974*
[2]*Physics Department, University of Konstanz, Konstanz, Germany*
(Received 11 December 2000)

Tl_9BiTe_6 exhibits a thermoelectric figure of merit of ZT $\sim$ 1.2 around 500 K, which significantly exceeds the state-of-the-art materials in this temperature range. The extraordinary thermoelectric performance is mainly due to the extremely low thermal conductivity of Tl_9BiTe_6 [0.39 W/(m $\cdot$ K) at 300 K]. In fact, the minimum lifetime of the phonons has to be taken into account to describe the thermal conductivity data.

DOI: 10.1103/PhysRevLett.86.4350 PACS numbers: 72.20.Pa, 66.70.+f

The efficiency of a thermoelectric device (cooler or generator) depends on the materials properties through the thermoelectric figure of merit $ZT = S^2T/(\rho\kappa)$, where S is the thermopower, T is the temperature, ρ is the electrical resistivity, and κ is the thermal conductivity. The thermopower and the resistivity are determined only by the electronic properties of the material and are thus often combined to a form S^2/ρ, which is called the "power factor." In contrast, the thermal conductivity $\kappa = \kappa_l + \kappa_e$ is composed of a lattice contribution (κ_l) and an electronic contribution (κ_e).

While the power factor can often be optimized by varying the carrier concentration of a material, the possibilities to reduce κ, especially κ_l, which is determined by the crystal structure and the bond strengths, are rather limited. Thus, the search for new thermoelectric materials is focusing on finding compounds with inherently low thermal conductivity as, for example, clathrates [i.e., $Sr_4Eu_4Ga_{16}Ge_{30}$ $\kappa_l = 0.6$ W/(m $\cdot$ K) [1]], filled skutterudites [i.e., $La_{0.75}Th_{0.2}Fe_3CoSb_{12}$, $\kappa_l =$ 1.2 W/(m $\cdot$ K) [2]], and complex bismuth telluride related materials [i.e., $CsBi_4Te_6$ $\kappa_l = 0.8$ W/(m $\cdot$ K) [3]], where the thermal conductivity is given at 300 K.

According to a model proposed by Slack [4] low thermal conductivity can be expected in compounds which have a low melting point, a large average mass of its constituent atoms, and a large unit cell. These criteria are well matched by the ternary compound Tl_9BiTe_6 [5]. In fact, κ as low as 0.75 W/(m $\cdot$ K) at 300 K has been reported previously for this compound [6]. The electronic contribution estimated from the Wiedemann-Franz law [1.6 m$\Omega \cdot$ cm $\rightarrow$ $\sim$0.4 W/(m $\cdot$ K) at 300 K] suggests that the lattice contribution is only between 0.3 and 0.4 W/(m $\cdot$ K).

Tl_9BiTe_6 belongs to a large group of ternary compounds which can be derived from the isostructural Tl_5Te_3. The binary compound is reported to be semimetallic [7]. As seen from the coordination polyhedra in Fig. 1, there are no Te-Te bonds in the structure since the nearest neighbors of the Te atoms are exclusively Tl atoms. Assuming that the three Te atoms in Tl_5Te_3 are in the valence state Te^{2-}, the five Tl atoms would have to provide six electrons. This is achieved by expanding the formula unit to $Tl^{1+}{}_9Tl^{3+}Te^{2-}{}_6$, where the $4c$ site, which accommodates two Tl atoms per expanded formula unit, is equally occupied by Tl^{1+} and Tl^{3+}.

Although this valence model is quite simple, it gives a very good description of the structure of the Tl_5Te_3 group, which is visualized in Fig. 2. The Tl^{3+} can be substituted with the trivalent elements Bi^{3+} and Sb^{3+}, resulting in the compounds with 9-1-6 stoichiometry. On the other hand,

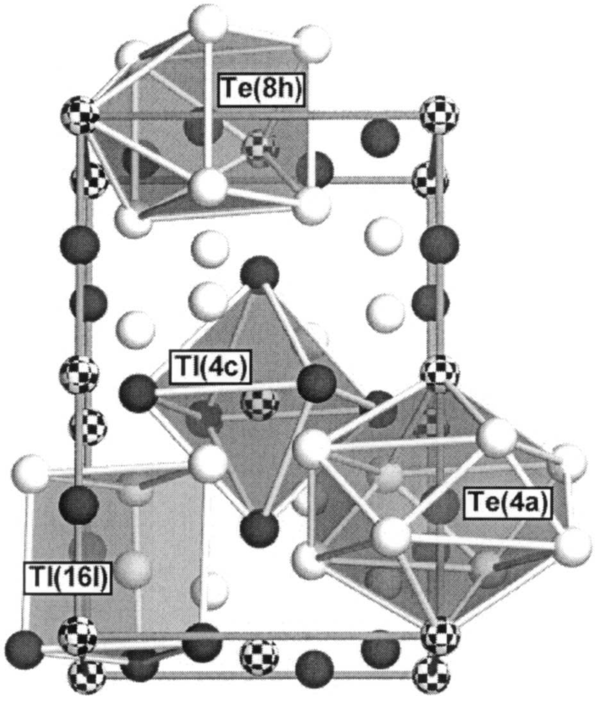

FIG. 1. The tetragonal unit cell of Tl_5Te_3 as seen perpendicular to the c axis. The four different crystal sites and their coordination polyhedra are shown. The tellurium atoms are depicted in black with the coordination for the $4a$ site and the $8h$ site shown in the lower right and on top, respectively. The thallium atoms are shown in white on the $16l$ site, coordination as in the lower left, and checkered on the $4c$ site, where they are octahedrally coordinated (center). In the ternary compounds the additional atoms are substituted on the $4c$ site.

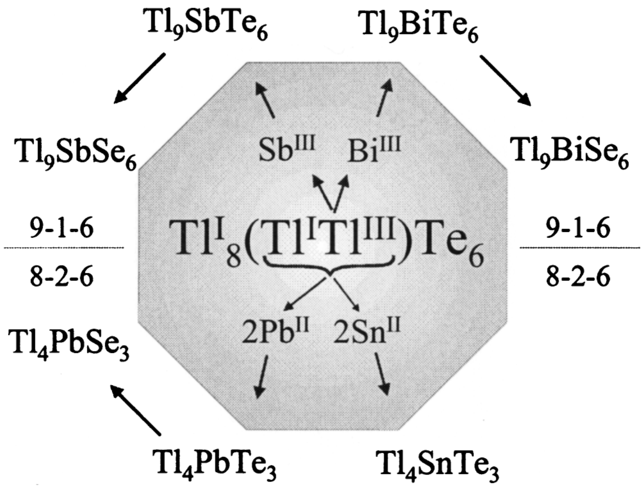

FIG. 2. The Tl_5Te_3 group and its ordered (8-2-6) and disordered (9-1-6) subgroups. The ternary compounds are derived from the expanded formula unit of Tl_5Te_3 by different substitutions.

since the $4c$ site is equally occupied by Tl^{1+} and Tl^{3+}, it can be understood as a site with an average valence of 2+. From this the 8-2-6 compounds are obtained by substituting the Tl^{1+} and the Tl^{3+} on the $4c$ site with two Pb^{2+} or two Sn^{2+}. Apart from $Tl_8Sn_2Se_6$ the corresponding selenides exist as well for all ternary compounds. Since the distribution of Tl and Bi (Sb) on the $4c$ site is random, we describe the 9-1-6 compounds as the disordered subgroup. The 8-2-6 subgroup is ordered since the $4c$ site is occupied by a single atomic species, Pb or Sn.

This large group of closely related compounds, which have been shown to be completely miscible [8], offers a wide phase space for optimization of the thermoelectric properties of these materials.

Because all compounds of the Tl_5Te_3 group melt congruently, they are obtained by direct synthesis of stoichiometric amounts of high purity elements (99.999% and better, metals basis) in evacuated quartz ampoules. As we have synthesized them, Tl_9BiTe_6 exhibits the highest power factor, $S^2/\rho = 0.46\ \mathrm{mW/(m \cdot K)}$, of all compounds in the Tl_5Te_3 group. Therefore, this compound has been chosen for further study. In order to improve the thermoelectric properties of Tl_9BiTe_6, the material is purified by zone refining in a horizontal configuration. A molten zone of 1 cm width is passed 3 times along an ingot of 10 cm length with a speed of 5 mm/h. The samples for transport measurements are cut from the middle of the ingot. The purified material is stable in air. Zone refining results in polycrystalline material with large grains (~1 cm). However, no significant anisotropy has been observed in the transport measurements.

The electrical properties of zone refined Tl_9BiTe_6 are shown in Fig. 3. The positive thermopower values indicate that holes are the dominant carriers in this material. The thermopower of Tl_9BiTe_6 increases monotonically with temperature and reaches a value of $399\ \mu\mathrm{V/K}$ at 500 K. Hall measurements [Figs. 3(B) and 3(D)] have been carried out in the temperature range from 20 to 340 K. From the measured resistivity and the Hall coefficient, the mobility, the effective Hall factor, and the hole concentration are calculated. The mobility data can be described very well with a model using two scattering mechanisms, where at low temperatures the mobility is limited by neutral impurity scattering, while acoustic phonon scattering becomes increasingly important at higher temperatures. The effective Hall factor is a weighted average regarding the two different scattering mechanisms. As a result, the hole concentration is found to be almost temperature independent with a value of approximately $2 \times 10^{19}\ \mathrm{cm}^{-3}$, whereas the mobility decreases from $700\ \mathrm{cm^2/(V \cdot s)}$ at 20 K to $62\ \mathrm{cm^2/(V \cdot s)}$ at 300 K. The power factor S^2/ρ of Tl_9BiTe_6 rises from the lowest temperatures to 200 K and is almost constant up to 500 K with a value of approximately $1\ \mathrm{mW/(m \cdot K^2)}$, which represents a 100% improvement over the as synthesized compound. While this is a very important improvement the power factor of Tl_9BiTe_6 is still low compared to other thermoelectric materials, i.e., Bi_2Te_3 [$\sim 4\ \mathrm{mW/(m \cdot K^2)}$].

The thermal conductivity of Tl_9BiTe_6 (see Fig. 4) has been measured using two different techniques. At temperatures below 140 K the longitudinal steady state method has been applied. At higher temperatures the thermal conductivity has been determined by the 3ω method [9], which is less susceptible to radiation losses. In the temperature overlap, from 80 to 140 K, the values of the two methods agree within a few percent. Calculating the electronic and the lattice contribution from the Wiedemann-Franz law shows that the thermal conductivity is primarily determined by the lattice. Between 200 and 250 K, where the electronic contribution is most relevant, it amounts only to approximately one-fifth of the total thermal conductivity.

A lower bound for the thermal conductivity of Tl_9BiTe_6 can be calculated using a model proposed by Slack [4]. The so called "minimum thermal conductivity" $\kappa_{\min}$ is the thermal conductivity expected for a completely disordered material with otherwise similar properties. It is calculated under the assumption that the minimum lifetime of a defined lattice vibrational mode is half the period of the vibration [10]. At 300 K the lattice contribution [$0.39\ \mathrm{W/(m \cdot K)}$], calculated from the Wiedemann-Franz law, is only slightly more than twice the expected minimum of $0.17\ \mathrm{W/(m \cdot K)}$. In fact, it can already be seen from the data that the thermal conductivity has a temperature dependence of the form

$$AT^{-x} + \kappa_{\min} \tag{1}$$

rather than being just proportional to T^{-x} as it is found in materials with higher thermal conductivity. This results from the fact that the phonon mean free path l is described by [11]

$$l = \left(\sum_i l_i^{-1}\right)^{-1} + l_{\min}\,, \tag{2}$$

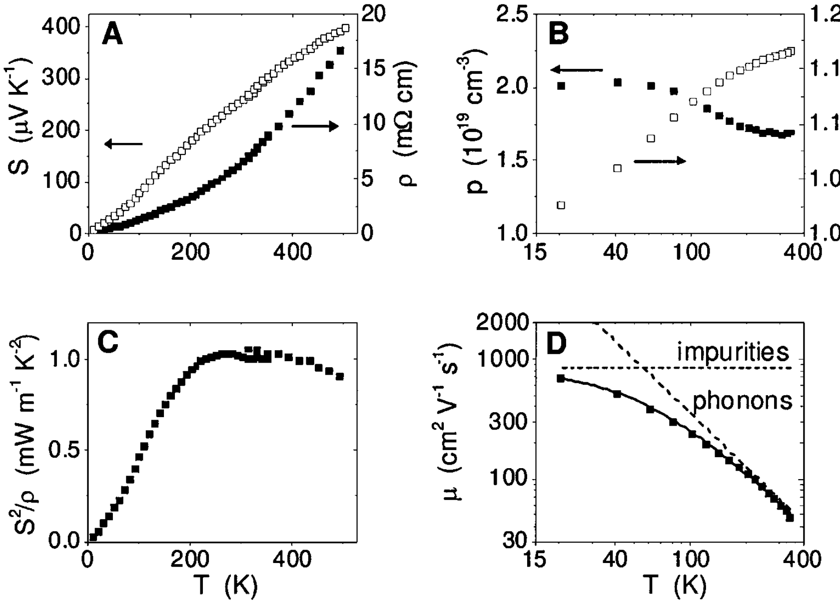

FIG. 3. (A) Thermopower and resistivity of zone refined Tl_9BiTe_6 as a function of temperature. There is a small offset between the low temperature and high temperature measurements in the thermopower data. (B) The effective Hall factor and the hole concentration as a function of temperature as calculated from the resistivity and the Hall coefficient. (C) The power factor S^2/ρ calculated from the thermopower and resistivity data. The offset in the power factor results from the thermopower measurements. (D) The hole mobility of Tl_9BiTe_6 as a function of temperature (squares) and a fit to the data (solid line) using a model with neutral impurity scattering and acoustic phonon scattering (dashed lines) as the relevant mechanisms.

where the i represent the contribution of the different scattering mechanisms, while the minimum mean free path $l_{\min}$ is a result of the minimum phonon lifetime as discussed above. In our case, where $\kappa \approx 2\kappa_{\min}$, the mean free path due to the different scattering mechanisms is comparable to the minimum mean free path $\sum_i l_i \approx l_{\min}$. A fit to the data using Eq. (1) yields $x = 0.93 \pm 0.1$ and $\kappa_{\min} = 0.21 \pm 0.03$ W/(m · K), where $\kappa_{\min}$ is in very good agreement with the calculated value.

The ordered compound $Tl_8Pb_2Te_6$, which has two Pb on the $4c$ site, exhibits a lattice thermal conductivity 0.72 W/(m · K) at 300 K, which is almost twice the value of Tl_9BiTe_6. The disorder on the $4c$ site has a very pronounced effect on the thermal conductivity, even though the mass difference between Tl and Bi is very small (~2%). For impurities on a single atomic site, the effect of point defect scattering due to mass differences depends on the parameter $\Gamma = \sum f_i(1 - M_i/M_{av})^2$, which reduces to $\Gamma = \alpha(1 - \alpha)(\Delta M/M_{av})^2$ for a single type of impurity atom with concentration α [12]. For typical examples from the field of thermoelectrics Γ is of the order of 10^{-2} ($Bi_{0.1}Sb_{0.9}$: 0.040; $Ge_{0.9}Si_{0.1}$: 0.038), while in the case of Tl_9BiTe_6 Γ equals 4.6×10^{-5}. Therefore, the mass difference between the two species Tl and Bi can be ruled out as an important scattering mechanism.

Presumably, the strong scattering results from the difference in the valence states on the $4c$ site, Bi^{3+} and Tl^{1+}, respectively. A very pronounced reduction of the lattice thermal conductivity in mixed-valence systems has already been observed in $Ru_{0.5}Pd_{0.5}Sb_3$ [13,14] and Fe_3O_4 [15]. It is suggested that the phonons induce a charge transfer between Ru^{4+}/Ru^{2+} and Fe^{3+}/Fe^{2+}, respectively. However, in the case of Tl_9BiTe_6 the mixed valence site is occupied by two different atom species Tl^{1+}/Bi^{3+}, thus making this system more complex. We expect more detailed insight

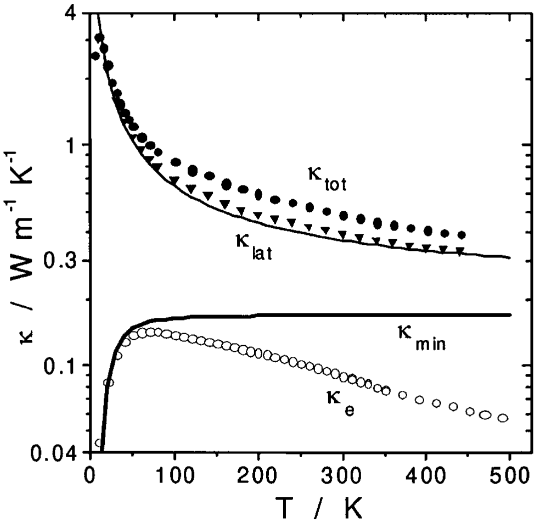

FIG. 4. The total thermal conductivity (full circles) of Tl_9BiTe_6 as a function of temperature as measured by the longitudinal steady state method and the 3ω technique. The electronic contribution (open circles) is calculated from the Wiedemann-Franz law and subtracted from the total thermal conductivity to obtain the lattice contribution (triangles). A fit to the data as described in the text is shown by the light line. The heavy line represents the minimum thermal conductivity, as calculated for a completely disordered solid with otherwise similar properties as Tl_9BiTe_6.

from $Tl_9BiTe_6/Tl_8Pb_2Te_6$ solid solutions which allow one to study the scattering mechanism as a function of the concentration of Tl^{1+}, Pb^{2+}, and Bi^{3+} on the $4c$ crystal site.

Assuming that $\kappa \propto l$ and neglecting the frequency dependence of the different scattering mechanisms, we can calculate the thermal conductivity which the material would exhibit if the disorder scattering were the only present mechanism. Under these conditions Eq. (2) translates to

$$\kappa = (\kappa_0^{-1} + \kappa_d^{-1})^{-1} + \kappa_{\min}, \quad (3)$$

where κ is the thermal conductivity of the disordered compound (Tl_9BiTe_6) and κ_0 is the thermal conductivity without the presence of disorder ($Tl_8Pb_2Te_6$). Then $\kappa_d + \kappa_{\min}$ is the thermal conductivity for a compound with disorder as the only scattering mechanism but otherwise equal properties. With $\kappa_{\min} = 0.2\ \mathrm{W/(m \cdot K)}$ a value of $\kappa_d + \kappa_{\min} = 0.58\ \mathrm{W/(m \cdot K)}$ is calculated, which is lower than the thermal conductivity of the ordered compound. This shows that the scattering due to the valence disorder is a very strong mechanism and we expect other materials with mixed valence states on one crystal site also exhibit low thermal conductivities.

In Fig. 5 the thermoelectric figure of merit of Tl_9BiTe_6 is compared to those of current state-of-the-art p-type materials [5,16–18]. Because of its very low thermal conductivity, at room temperature the figure of merit of Tl_9BiTe_6 ($ZT = 0.65$) is already equal to that of pure p-type Bi_2Te_3, but Tl_9BiTe_6 is still less efficient than $Bi_{2-x}Sb_xTe_{3-y}Se_y$ alloys ($ZT \sim 1$). However, because of the larger band gap, $E_g \geq 0.4$ eV in Tl_9BiTe_6 compared to $E_g \sim 0.15$ eV in Bi_2Te_3 [16], the optimum operating temperature of Tl_9BiTe_6 is at higher temperatures. Above 430 K the thermoelectric figure of merit of Tl_9BiTe_6 is greater than 1 and it outperforms optimized $Bi_{2-x}Sb_xTe_{3-y}Se_y$ alloys. Around 500 K Tl_9BiTe_6, with $ZT \sim 1.2$, significantly exceeds the thermoelectric efficiency of optimized $Bi_{2-x}Sb_xTe_{3-y}Se_y$ and $(GeTe)_{85}(AgSbTe_2)_{15}$ alloys, so called TAGS-85, both with $ZT \sim 0.8$.

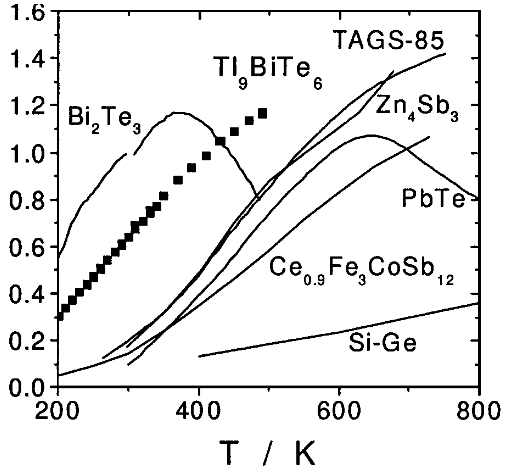

FIG. 5. The thermoelectric figure of merit ZT of Tl_9BiTe_6 as a function of temperature (squares) compared to those of state-of-the-art p-type materials.

While the thermoelectric properties of Tl_9BiTe_6 were greatly improved by zone melting, a systematic study of doping the p-type compound has not yet been carried out and further improvements can be expected. The extremely low thermal conductivity is the key property that leads to the very high figure of merit of Tl_9BiTe_6. More detailed understanding of the lattice vibration properties of this compound would be of significant scientific interest and would also serve to guide further thermoelectric research.

One of the authors (B. W.) gratefully acknowledges financial support by the Deutsche Akademische Austauschdienst (DAAD).

---

*To whom correspondence should be addressed.
Electronic address: woe@lucent.com

[1] J. L. Cohn, G. S. Nolas, V. Fessatidis, T. H. Metcalf, and G. A. Slack, Phys. Rev. Lett. **82**, 779 (1999).
[2] B. C. Sales, D. Mandrus, B. C. Chakoumakos, V. Keppens, and J. R. Thompson, Phys. Rev. B **56**, 15 081 (1996).
[3] D.-Y. Chang *et al.,* Science **287**, 1024 (2000).
[4] G. A. Slack, in *Solid State Physics: Advances in Research and Applications,* edited by H. Ehrenreich, F. Seitz, and D. Turnbull (Academic, New York, 1979), Vol. 34, pp. 1–73.
[5] I. E. Barchii, V. B. Lazarev, E. Yu. Peresh, Yu. V. Voroshilov, and V. I. Tkachenko, Izv. Akad. Nauk SSSR, Neorg. Mater. **24**, 1791 (1988) [Inorg. Mater. (USSR) **24**, 1526 (1988)].
[6] A. Pradel, J.-C. Tedenac, D. Coquillat, and G. Brun, Rev. Chim. Miner. **19**, 3 (1982).
[7] A. A. Toure, G. Kra, R. Eholie, J. Olivier-Fourcade, and J.-C. Jumas, J. Solid State Chem. **87**, 229 (1990).
[8] M. B. Babanly, A. G. Ali, and A. A. Kuliev, Izv. Akad. Nauk SSSR, Neorg. Mater. **15**, 1292 (1979) [Inorg. Mater. (USSR) **15**, 1011 (1979)]; Z. M. Latypov, N. R. Faizullina, R. N. Sagitov, and V. P. Savel'ev, Izv. Akad. Nauk SSSR, Neorg. Mater. **24**, 1920 (1988) [Inorg. Mater. (USSR) **24**, 1644 (1988)].
[9] D. G. Cahill, Rev. Sci. Instrum. **61**, 802 (1990).
[10] D. G. Cahill, S. K. Watson, and R. O. Pohl, Phys. Rev. B **46**, 6131 (1992).
[11] G. S. Nolas, T. R. Weakley, J. L. Cohn, and R. Sharma, Phys. Rev. B **61**, 3845 (2000).
[12] G. P. Meisner, D. T. Morelli, S. Hu, J. Yang, and C. Uher, Phys. Rev. Lett. **80**, 3551 (1998).
[13] T. Caillat, J. Kulleck, A. Borshchevsky, and J.-P. Fleurial, J. Appl. Phys. **79**, 8419 (1996).
[14] G. S. Nolas, V. G. Harris, T. M. Tritt, and G. A. Slack, J. Appl. Phys. **80**, 6304 (1996).
[15] G. A. Slack, Phys. Rev. **126**, 427 (1962).
[16] W. M. Yim and F. D. Rosi, Solid State Electron. **15**, 1121 (1972); D. A. Wright, Metall. Rev. **15**, 147 (1970).
[17] *CRC Handbook of Thermoelectrics,* edited by D. M. Rowe (CRC Press, Boca Raton, FL, 1995), Chaps. 21, 22, and 28, and references therein.
[18] T. Caillat, J.-P. Fleurial, and A. Borshchevsky, J. Phys. Chem. Solids **58**, 1119 (1997).